DR2005088

Table DR1: K-Ar and $^{40}Ar/^{39}Ar$ isotopic dating for the adakitic volcanic rocks and olivine-bearing leucite foidites in the Hohxil area

sample	Rock type	location	Dating method	Age (Ma)
3302	trachyte	Wuxuefeng	K-Ar	18.4 ± 0.4
3302-1	trachyte	Wuxuefeng	K-Ar	18.6 ± 0.4
3304-3b	trachyte	Hongshuihe	K-Ar	18.0 ± 0.4
3303	trachyte	Wuxuefeng	$^{40}Ar/^{39}Ar$	16.68 ± 0.44
3304-2	trachyte	Hongshuihe	$^{40}Ar/^{39}Ar$	16.38 ± 0.69
6304a	olivine-bearing leucite foidites	Southern Hohxil Lake	$^{40}Ar/^{39}Ar$	16.47 ± 1.22

K-Ar ages were determined at Laboratoire de géochronologie et UA 1278, Université de Bretagne Occidentale in France. Analytical procedures for K-Ar dating are similar to those described in detail by Defant et al. (1992). The results of $^{40}Ar/^{39}Ar$ dating are plateau ages. Argon isotope analyses were conducted on a MM-1200 mass spectrometer at the Laboratory of analyzing center, Guilin resource and geological institute. $^{40}Ar/^{39}Ar$ dating experimental procedures were described in detail by Dai and Hong (1982) and Wang et al. (2002).

References cited

Dai, T.M., and Hong, A.S., 1982, $^{40}Ar/^{39}Ar$ dating and some isotopic determinations on Himalaya biotites from granitoids rocks in southern Tibet: Geochimica, v. 11, p. 48—55 (in Chinese with English abstract).

Defant, M.J., Jackson, T.E., Drummond, M.S., De Boer, J.Z., Bellon, H., Feigenson, M.D., Maury, R.C., and Stewart, R.H., 1992, The geochemistry of young volcanism throughout western Panama and southeastern Costa Rica: an overview: Journal of the Geological Society, London, v.149, p.569-579.

Wang, J.H., Yin, A., Harrison, T.M., Grove, M., Zhou, J.Y., Zhang, Y.Q., and Xie, G.Y., 2003, Thermochronological constraints on two pulses of Cenozoic high-K magmatism in eastern Tibet: Science in China, Series D, v. 46, p.719-729.

Table DR2: Major (wt%) and trace elements (ppm) concentrations for the Hohxil K-rich adakitic rocks and olivine-bearing leucite foidite

Areas	Wuxuefeng							Hongshuihe				Southern Hohxil Lake
sample	3302	3302-1	3302-2	3303	3303-1	3P$_1$1-1	3P$_1$2-1	3304-1	3304-2	3304-3a	3304-3b	6304a
SiO_2	61.28	62.81	62.38	63.20	66.81	63.11	63.8	65.43	66.0	65.12	66.95	44.82
TiO_2	1.16	1.09	1.13	1.12	0.77	1.08	1.04	0.94	0.89	0.94	0.87	1.46
Al_2O_3	16.57	15.28	15.73	15.66	14.35	15.58	14.79	16.26	15.55	16.42	15.24	12.18
Fe_2O_3	5.23	4.83	5.49	5.01	4.51	4.99	5.33	2.99	4.32	4.30	3.89	9.10
MnO	0.03	0.07	0.05	0.05	0.06	0.07	0.07	0.05	0.02	0.02	0.02	0.16
MgO	1.78	2.33	2.14	1.76	1.77	2.39	2.24	0.70	0.62	0.77	0.73	7.94
CaO	3.90	4.12	3.87	3.75	3.14	4.18	3.51	2.92	2.72	2.72	2.49	10.41
Na_2O	3.99	3.81	3.69	3.77	3.38	3.73	3.47	3.69	3.50	3.72	3.44	3.43
K_2O	4.68	4.25	4.34	4.16	4.02	4.16	4.16	4.47	4.43	4.48	4.14	6.05
P_2O_5	0.35	0.42	0.38	0.40	0.26	0.33	0.16	0.28	0.32	0.30	0.27	2.52
LOI	1.06	1.42	0.83	0.92	0.46	0.52	0.89	2.05	1.88	1.95	2.01	1.31
Σ	100.02	100.43	100.03	99.80	99.52	100.15	99.42	99.78	100.20	100.74	100.05	99.37
Mg#	40	49	44	41	44	49	45	32	22	26	27	63
Sc	7.87	8.26	8.67	8.15	8.49	10.7	9.43	6.25	7.80	6.87	5.92	25.5
V	83.1	75.2	80.2	77.2	66.7	72.6	64.4	44.2	69.7	69.6	70.0	154
Cr	50.2	47.6	42.2	47.7	40.0	43.6	49.5	38.3	43.6	48.2	47.4	149
Co	9.24	13.8	12.2	9.82	9.88	12.9	13.1	5.54	4.84	4.02	4.15	34.8
Ni	23.4	21.7	28.6	21.6	23.5	25.2	35.9	14.6	14.4	12.9	13.3	109
Rb	197	193	181	183	217	183	181	212	203	211	213	186
Sr	1009	966	932	1036	680	962	933	828	839	837	827	3266
Y	14.0	16.5	16.5	14.9	14.0	15.3	11.1	11.8	10.9	11.5	11.3	39.0
Zr	399	378	330	344	393	307	229	317	373	357	354	605
Nb	32.2	30.6	29.3	31.6	17.7	30.4	30.0	23.2	22.7	22.9	22.9	58.2
Ba	1548	1568	1422	1618	1423	1501	1477	1632	1633	1623	1595	4701
Hf	9.56	8.87	7.94	8.31	9.82	7.64	5.64	8.83	9.78	9.46	9.45	13.0
Ta	1.98	1.79	1.67	1.56	0.96	1.77	1.61	1.20	1.15	1.23	1.12	3.64
Pb	27.1	39.2	48.7	21.1	33.0	29.2	20.7	22.3	18.2	20.2	21.5	13.7
Th	51.8	52.2	49.4	49.5	60.2	45.1	40.3	57.4	53.9	56.5	56.5	20.6
U	5.71	7.06	6.43	4.67	7.03	6.48	4.71	4.88	3.31	4.37	4.50	4.07
La	116.5	132.5	122.5	118.3	124.7	110.4	81.4	119.7	110.8	110.5	106.6	212.2
Ce	193.6	220.7	209.0	219.6	252.1	190.9	139.3	242.0	189.2	189.7	189.0	452.2
Pr	21.76	24.77	23.71	22.79	24.49	21.55	14.40	23.22	20.95	21.37	20.72	53.4
Nd	71.49	82.76	76.22	77.11	79.94	72.13	47.23	74.68	68.83	69.42	67.15	209.1
Sm	9.02	10.11	9.38	9.59	9.53	9.04	6.09	8.98	8.38	8.48	8.06	30.65
Eu	2.33	2.26	2.19	2.16	1.69	2.09	1.72	1.83	1.83	1.84	1.88	6.61
Gd	4.96	5.76	5.17	4.59	3.88	4.16	3.02	3.69	3.55	3.52	3.62	15.91
Tb	0.71	0.79	0.73	0.64	0.55	0.59	0.41	0.52	0.47	0.50	0.48	2.02
Dy	3.37	3.74	3.62	3.15	2.90	3.25	2.31	2.56	2.48	2.61	2.50	9.04
Ho	0.55	0.62	0.62	0.53	0.50	0.55	0.40	0.42	0.40	0.43	0.42	1.40
Er	1.38	1.56	1.59	1.31	1.25	1.34	1.01	1.03	1.02	1.06	1.00	3.26
Tm	0.19	0.22	0.23	0.19	0.18	0.19	0.15	0.14	0.14	0.14	0.14	0.42
Yb	1.13	1.36	1.41	1.10	1.11	1.20	0.97	0.81	0.85	0.88	0.85	2.55
Lu	0.17	0.21	0.21	0.18	0.18	0.19	0.15	0.13	0.13	0.13	0.13	0.39
Eu/Eu*	1.07	0.91	0.96	0.99	0.85	1.04	1.23	0.97	1.02	1.03	1.06	0.92
Sr/Y	72	59	57	70	49	63	84	70	77	73	73	84
La/Yb	103	97	87	108	112	92	84	149	130	125	125	83

Major element oxides (wt%) were determined using a Varian Vista PRO ICP-AES at the Guangzhou Institute of Geochemistry, Chinese Academy of Sciences. The details of the analytical procedures were described by Li et al. (2002). Trace elements (ppm) were analyzed by a Perkin-Elmer Sciex ElAN 6000 ICP-MS at the Guangzhou Institute of Geochemistry, Chinese Academy of Sciences following procedures described by Liu et al. (1996). Analytical precision for most elements is better than 5%.

References Cited

Li, X.H., Liu, Y., Tu, X., Hu, G., and Zeng, W., 2002, Precise determination of chemical compositions in silicate rocks using ICP-AES and ICP-MS: A comparative study of sample digestion techniques of alkali fusion and acid dissolution: Geochimica, v. 31, p. 289-294 (in Chinese with English abstract).

Liu, Y., Liu, H.C., and Li, X.H., 1996, Simultaneous and precise determination of 40 trace elements in rock samples by ICP-MS: Geochimica, v. 25, p. 552-558 (in Chinese with English abstract).

Table DR3: Sr-Nd isotope ratios for the Hohxil K-rich adakitic rocks

sample	$^{87}Sr/^{86}Sr$	error	$^{143}Nd/^{144}Nd$	error	εND(t)	T_{DM}(Ga)
3302*	0.707428	0.000042	0.512418	0.000016	-4.29	0.81
3302 repeat*			0.512413	0.000024	-4.39	0.82
3302-1*	0.707253	0.000064	0.512413	0.000024	-4.39	0.81
3302-1 repeat*			0.512447	0.000030	-3.73	0.77
$3P_1$1-1	0.707351	0.000014	0.512443	0.000010	-3.80	0.78
$3P_2$2-1	0.707429	0.000013	0.512444	0.000010	-3.78	0.80
3303	0.707307	0.000014	0.512431	0.000010	-4.04	0.79
3304-1	0.707283	0.000016	0.512531	0.000011	-2.09	0.67
3304-2*	0.707457	0.000050	0.512432	0.000018	-4.02	0.78
3304-2 repeat*	0.707440	0.000036				
3304-3a	0.707211	0.000014	0.512470	0.000010	-3.28	0.74
3304-3b*	0.707368	0.000056	0.512403	0.000014	-4.58	0.81

* Denotes samples analyzed at University College Dublin, Ireland. The $^{87}Sr/^{86}Sr$ ratio of the NBS987 standard and $^{143}Nd/^{144}Nd$ ratio of the La Jolla standard measured during this study were 0.71030 ±3 ($2\sigma_m$) and 0.511830±15 ($2\sigma_m$), respectively. Sr and Nd isotopic compositions of other samples were measured by a Micromass Isoprobe multi-collector mass spectrometer (MC-ICPMS) at the Guangzhou Institute of Geochemistry, Chinese Academy of Sciences. Analytical procedures are similar to that described by Wei et al. (2002) and Liang et al. (2003). The $^{87}Sr/^{86}Sr$ ratio of the NBS987 standard and $^{143}Nd/^{144}Nd$ ratio of the JNdi-1 standard measured were 0.710288±28 ($2\sigma_m$) and 0.512109±12 ($2\sigma_m$), respectively. All measured $^{143}Nd/^{144}Nd$ and $^{86}Sr/^{88}Sr$ ratios are fractionation corrected to $^{143}Nd/^{144}Nd$ = 0.7219 and $^{86}Sr/^{88}Sr$ = 0.1194, respectively.

Liang, X.R., Wei, G.J., Li, X.H., and Liu, Y., 2003, Precise determination of $^{143}Nd/^{144}Nd$ and Sm/Nd ratios using multiple-collector inductively coupled plasmamass spectrometer (MC-ICPMS): Geochimica, v.32, p. 91-96 (in Chinese with English abstract).

Wei, G.J., Liang, X. R., Li, X. H., and Liu, Y., 2002. Precise measurement of Sr isotopic composition of liquid and solid base suing (LP) MC-ICPMS. Geochimica, v.31, p. 35-42 (in Chinese with English abstract).

Table DR4: composition of starting materials (source rocks) for partial melting model calculations

sample rocks	K89G185 Shoshonite	LH01-8 Garnet-bearing amphibolite xenolith
SiO_2	51.42	47.40
TiO_2	1.85	1.62
Al_2O_3	14.62	10.93
Fe_2O_3	9.61	3.67
FeO		3.67
MnO	0.14	0.21
MgO	4.03	12.3
CaO	7.59	8.8
Na_2O	4.60	1.25
K_2O	4.77	2.07
P_2O_5		0.2
CO_2		
H_2O		
LOI	2.09	3.87
La	177	22.89
Sm	20.2	8.68
Eu	4.3	2.2
Yb	1.5	6.69
Lu	0.2	0.93
Y	32	52.2
U	3	
Th	27	
References	Turner et al. (1996)	Wei (2002)

Turner, S., Arnaud, N., Liu, J., Rogers, N., Hawkesworth, C., Harris, N., Kelley, S., van Calsteren, P., and Deng, W., 1996, Postcollision, shoshonitic volcanism on the Tibetan plateau: Implications for convective thinning of the lithosphere and the source of ocean island basalts: Journal of Petrology, v. 37, p. 45–71.

Wei, Q.R., 2002, Petrology and geochemistry of the Xenoliths from Cenozoic two-pluse high-K magmatic rocks in eastern Tibet. The postdoctoral researches report of Guangzhou Institute of Geochemistry, Chinese Academy of Sciences. P.1-116 (in Chinese with English abstract).

Figure DR 1 and 2 captions

Figure DR1. La/Yb vs La diagram for the Hohxil K-rich adakitic rocks and shoshonitic mafic volcanic rocks (SiO_2 <55%) in Tibet. The Hohxil K-rich adakitic rocks plot in the partial melting array, but the shoshonitic mafic rocks (SiO_2<55%) from Tibet (Turner et al., 1996; Miller et al., 1999) plot on a different partial melting array. Thus, the figure clearly indicates that magmas of these shoshonitic mafic rocks cannot be parental to the K-rich adakitic rocks, and they are not related by fractional crystallization. Data for the Cenozoic shoshonitic volcanic rocks of Tibet are after Turner et al., (1996) and Miller et al., (1999).

Figure DR2. Results of modeling partial melting by using different source rocks (garnet-bearing amphibolite xenoliths and shoshonite in northern Tibet). A: Results from a batch partial melting model using a hypothetical garnet-bearing amphibolite source rock based on a crustal xenolith from Tibet, with compositions after Wei (2002). F is the melt fraction. Dashed lines represent the Hohxil K-rich adakitic rock compositional field. Th and U concentrations are not available for the xenolith, and so the model results do not include these elements. Mineral proportions in the source are based on the modal mineralogy of the xenolith. Modeled melts have REE contents similar to the Hohxil K-rich adakitic rocks. B: Results from a batch partial melting model using a Tibetan shoshonite (sample K89G185) as a hypothetical source rock, with compositions after Turner et al. (1996). F is partial melt fraction. Dashed lines represent the Hohxil K-rich adakitic rock compositional field. Mineral proportions in the model source are based on the shoshonite modal mineralogy. Modeled melts have HREE and U, Th, Y element concentrations quite different from the Hohxil K-rich adakitic rocks.

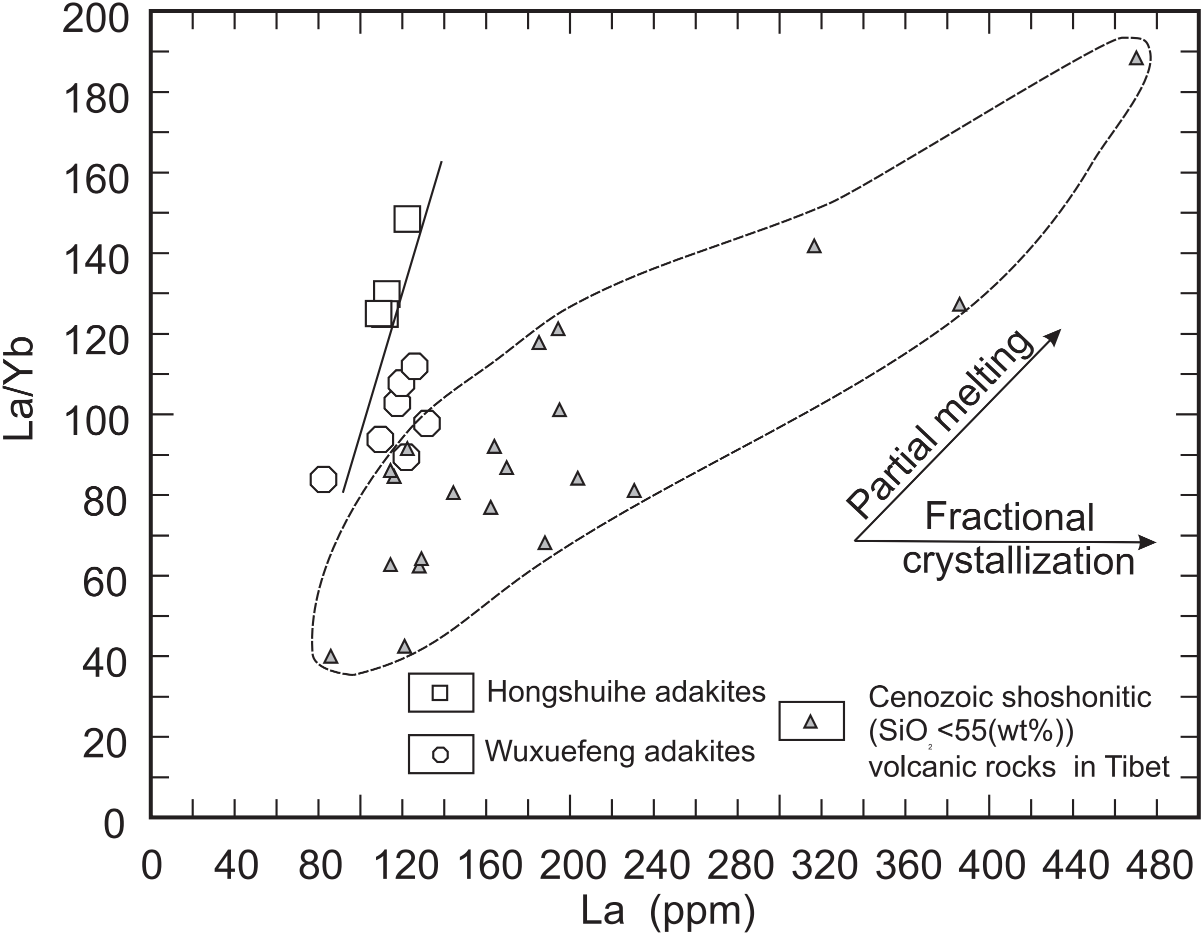

G21522-Fig-DR-1

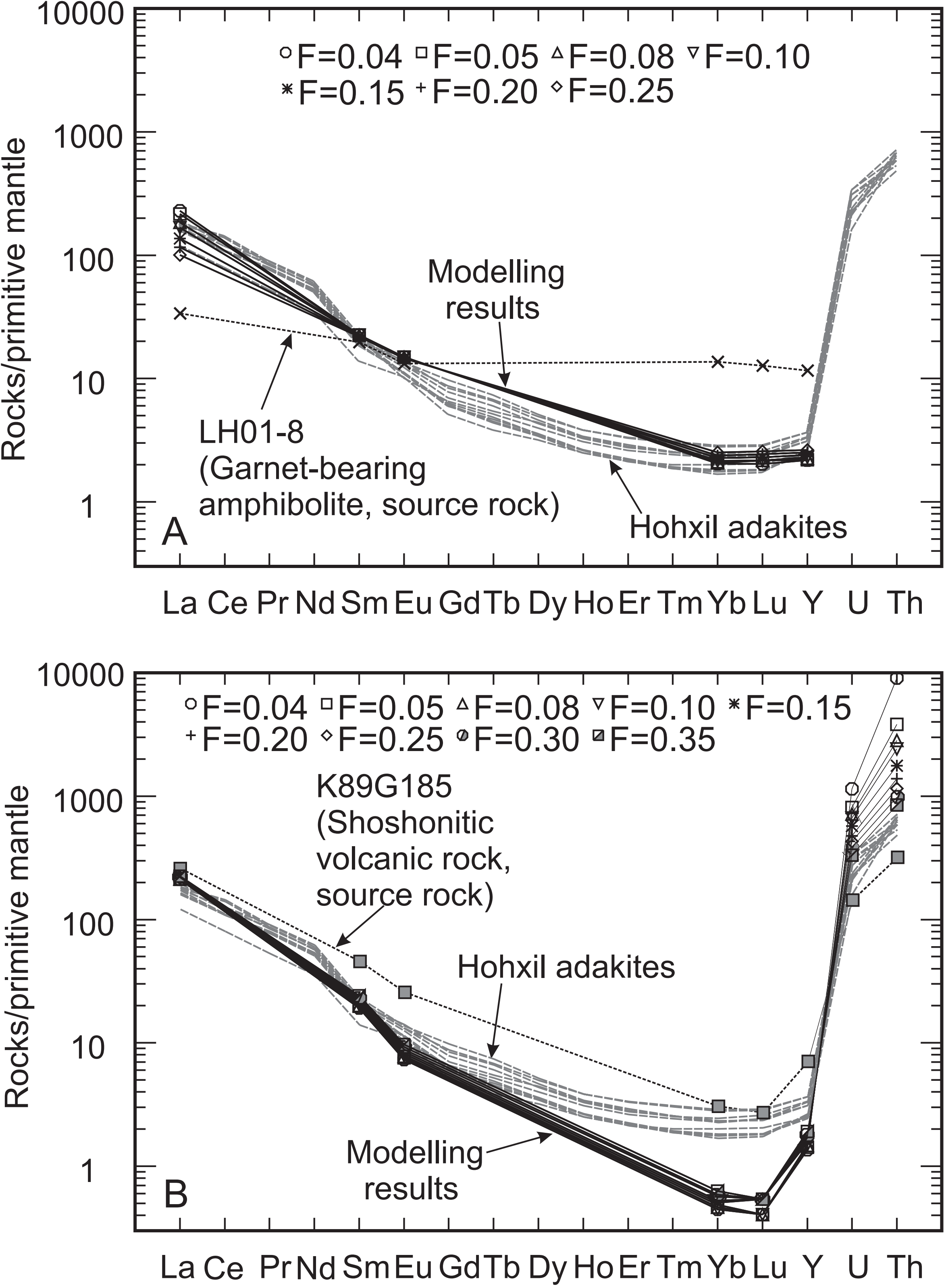

G21522-Fig-DR-2